COMBINED IMPACT OF INHERENT AND STRESS-INDUCED ANISOTROPY ON ROCK PERMEABILITY AND SLOPE STABILITY: ODA'S EQUATION SOLUTION AND FLAC3D SIMULATION ANALYSIS

CHIA-HUEI TU[1], JIA-JYUN DONG[2], ALVIAN RIZKY YANUARDIAN[3], JIA-YI WU[4]

[1] *Graduate Institute of Applied Geology, National Central University, Taiwan, tu_758594520@hotmail.com*

[2] *Graduate Institute of Applied Geology, National Central University, Taiwan, jjdong@geo.ncu.edu.tw*

[3] *Graduate Institute of Applied Geology, National Central University, Taiwan, alvian.ry@gmail.com*

[4] *Graduate Institute of Applied Geology, National Central University, Taiwan, jweek44@gmail.com*

Introduction

The joints within the rock mass can also become pathways for groundwater flow, and pore water pressure can reduce the effective stress and shear strength of potential sliding surfaces. Groundwater can accelerate rock weathering and reduce strength, all of which negatively impact the stability of rock slopes. Oda (1985) selected appropriate boundary conditions based on analytical conditions, defined system boundaries, and considered saturated groundwater flow in mountainous areas, classifying groundwater flow systems into small-scale, medium-scale, and large-scale types. Wyllie and Chris (2004) assumed that the slope material is composed of sedimentary material, suggesting that horizontal permeability might be higher than vertical permeability. This indicates that permeability anisotropy has a certain degree of influence on slope pore water pressure and the steady-state flow system of groundwater. Dong et al. (2006) used an equivalent concept to explore the impact of permeability anisotropy on the distribution of pore water pressure in rock slopes. Furthermore, pore water pressure affects the shear strength and effective stress of potential sliding surfaces, further influencing slope stability. However, secondary fractures and stress-induced permeability anisotropy in the rock mass have not yet been considered. Therefore, further research is needed on the influence of joint orientations in the rock mass or joint closures due to stress on the stability of jointed rock slopes (Dong et al., 2012).

Methods

This study discusses the impact of two conditions on slope stability: inherent joints and stress-induced anisotropic permeabilities. A numerical model of a rock slope was designed using FLAC3D, and the stress field was solved through gravity equilibrium. The stress data from the model grid were imported into Oda's equation to calculate the anisotropic permeability tensor. This tensor was then substituted back into the FLAC3D model to solve for the pore water pressure distribution, and the slope stability was analysed using the shear strength reduction method. In Condition 1, we assumed that the permeability is influenced by the distribution of multiple sets of joints. This study reflected the degree of difference in joint density in each direction using the coefficients $D_{X'X'}$, $D_{Y'Y'}$, and $D_{Z'Z'}$ of the fabric tensor, and assumed a higher density for joints parallel to the slope surface (bedding parallel joints). In Condition 2, we considered the directionality of the principal stress distribution, with the maximum principal stress parallel to the slope surface and the minimum principal stress perpendicular to the slope surface. Various stress ratios (maximum principal stress/minimum principal stress = 1 to 5) were also assumed.

Results

Assuming a homogeneous isotropic analysis as the control group, the results are shown at the top of Figure 1. Figures 2(b) and 1(a) (middle) display permeability tensor distributions for Condition 1 ($D_{Z'Z'}$ =0 to 4) and Condition 2 (stress ratios = 1 to 5). Without considering stress direction, the minimum permeability tensor remains horizontal, while it aligns parallel to the slope when stress ratio is considered. Figure 2(a) shows permeability coefficient variations. For Condition 1 (blue line), the maximum permeability tensor increases with $D_{Z'Z'}$, while the minimum decreases. For Condition 2 (orange line), both increase with stress ratio. Figure 2(b) indicates that Condition 1 has a greater impact on permeability anisotropy than Condition 2, with a maximum value of 7 times versus 1.44 times.

Figure 1(b) presents pore pressure distributions for isotropy, Condition 1 ($D_{Z'Z'}$ =4), and Condition 2 (stress ratio = 5). Pore pressure distribution is significantly influenced by permeability anisotropy; Condition 2 shows little difference from isotropy due to lower anisotropy. Figure 2(c) shows safety factor results, mirroring trends in Figure 2(b). For Condition 1, the safety factor increases with anisotropy, while for Condition 2, it converges. Figure 1(c) illustrates maximum shear strain increments for isotropy, Condition 1 ($D_{Z'Z'}$ =4), and Condition 2 (stress ratio = 5). Higher shear strain increments occur at the slope toe, especially in Condition 1 with higher permeability anisotropy. However, the safety factor for Condition 1 is also relatively larger.

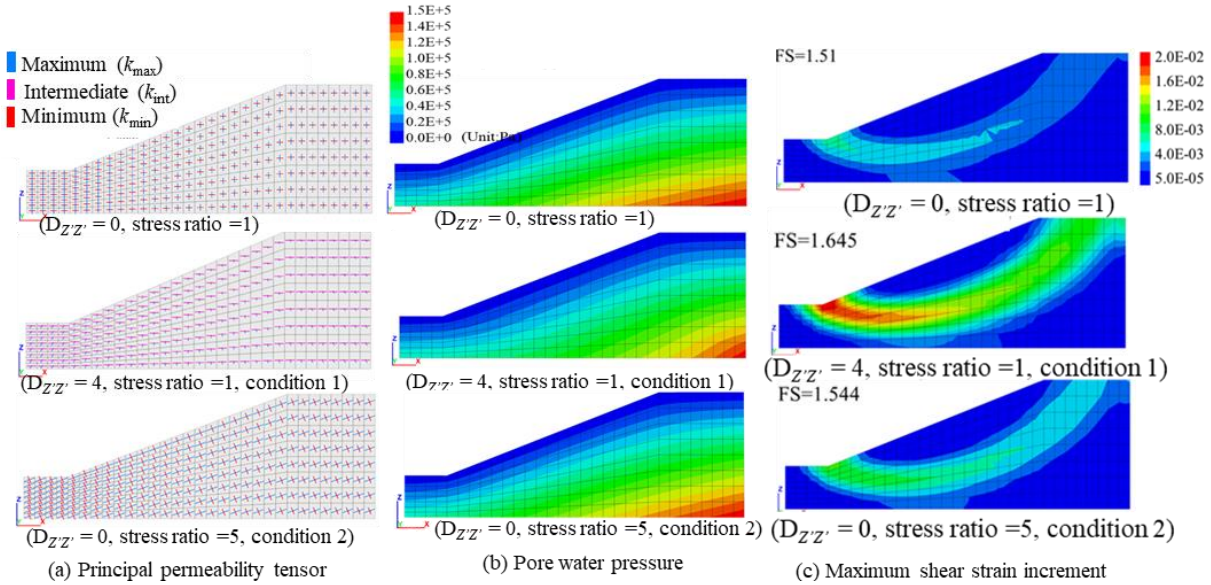

Figure 1. The distribution of permeability tensors, pore water pressure, and maximum shear strain increment for each condition.

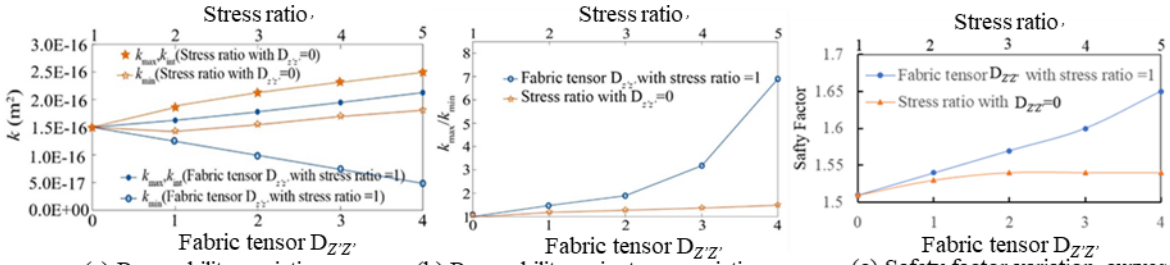

Figure 2. The permeability variation curves, permeability anisotropy variation curves, and safety factor variation lines for each condition.

Conclusion

This study simplified the analysis by treating stress and joint distribution as separate conditions. It aimed to compare their impact on permeability anisotropy. Results suggest that joint distribution has a stronger influence on permeability anisotropy when stress isn't considered. However, in Condition 2, where joint distribution remains constant, changes in permeability anisotropy are minimal.

References

Dong, J.J.; Tu, C.H.; Lee, W.R.; Jheng, Y.J. Effects of hydraulic conductivity/strength anisotropy on the stability. *Computers and Geotechnics*. 2012, 40, 147-159.

Dong, J.J.; Tzeng, J.H.; Wu, P.K.; Lin, M.L. Effects of anisotropic permeability on stabilization and pore water pressure distribution of poorly cemented stratified rock slopes. *International Journal for Numerical and Analytical Methods in Geomechanics*. 2006, 30(15), 1501-1600.

Oda, M. Permeability tensor for discontinuous rock masses. *Geotechnique*. 1985, 35(4), 483-495.

Wyllie, D.C.; Chris, M. *Rock Slope Engineering Civil and Mining*, In: Hoek, E. & Bray, J.W., Eds., Rock Slope Engineering, London, 2004.

MULTI-TEMPORAL EVALUATION OF LANDSLIDES IN A DAM RESERVOIR AREA WITH THE INTEGRATION OF MULTIPLE METHODS

TÜMAY KADAKCİ KOCA [1]

[1] *Muğla Sıtkı Koçman University, Geological Engineering Department, Türkiye, tumaykoca@gmail.com*

Introduction

The landslides in the reservoir area of dam sites necessitate profound geological and geotechnical investigations since any mass movement after dam construction may cause catastrophic damage to the engineering project. Detailed geological and geotechnical investigation of reservoir slopes and generating engineering geological models and a time-dependent mechanical approach are crucial for hazard mitigation. To date, several research have evaluated the stability of the reservoir slopes separately by the combination of field works and numerical or limit equilibrium models (Luo et al. 2019; Kafle et al. 2022). On the other hand, some of them studied with the combination of field works and remote sensing techniques (Iqbal et al. 2017; Gan et al. 2019). In general, extensive laboratory testing on rock/soil material is lacking. On the contrary, laboratory testing has been combined with numerical or limit equilibrium models to determine the stability conditions in several studies (Sun et al. 2016; Wang et al. 2022). To the best of author's knowledge, there is no multi-temporal study on the stability of reservoir slopes with the combination of different field investigations, laboratory tests, and remote sensing techniques. This study therefore aims to (i) determine the topographical evolution over time (ii) construct an engineering geological model explaining the mechanism of the landslides (iii) estimate the volume and sliding rate of landslides (iv) determine the role of triggering factors (e.g., seismic activity, heavy rainfall, wildfire) in the Miocene sedimentary rock slopes in the reservoir area.

Methods

A multi-method approach was adapted to achieve the scope of this study. Firstly, field investigations such as borehole logging, discontinuity measurement according to ISRM (2007), and geophysical survey (MASW and ERT) were performed. Secondly, laboratory works such as static and cyclic mechanical testing (uniaxial compressive and shear tests) have been performed under dry and water-saturated conditions. Afterward, photogrammetric analyses by using multi-temporal (1953-2017) aerial photographs in conjunction with the back analyses of numerical models were conducted. The purpose of using the photogrammetric results in the back analyses is to simulate the real slopes more accurately. photogrammetric displacement-based back analyses of the failed slopes have been performed by utilizing the finite element method (FEM). Numerical modeling of slopes is a useful tool to corroborate or develop the interpretation of slope behavior; however, a proper evaluation of the field observations, geological and hydrological data, as well as the physical, mechanical, and deformation properties of the rock mass is the key issue for realistic slope model. In this manner, static and cyclic laboratory tests and in-situ tests were performed.

Results

Initially, geological cross-sections passing through landslides were constructed to illustrate the main geostructural features and lithological units in the study area (Figure 1). Afterward, an engineering geological model (EGM) was constructed for the landslides in the study area based on the inferences from field observations, geophysical investigations, cored boreholes, photogrammetric analysis, and stereographic projection. The EGM provided a good understanding of the mechanism and possible time-dependent response of soil and rock units (Kadakci Koca 2021). Soil and rock materials have been depleted from the four slopes between 1953 and 2012 with an average mobilization rate of 2.06 x104 m^3/year. Hence, the landslides in the study area can be characterized by continuous movement with fluctuations in sliding rate (2012-1995: $1.37x10^4$ m^3/year, 1995-1953: $2.34x10^4$ m^3/year) due to different triggering factors. The seismic activity in 1969 was found to be the most significant triggering factor, inducing the largest material movement. It is also apparent that after the wildfire occurred in 1988, the cohesive strength of vegetation roots was lost and therefore the erosional process accelerated and

through a long period it promoted an overall decrease in shear strength in the soil mantle and the weathered and weak rock layers. Rainfall events, principally after the wildfire facilitated the transportation of granular material and played a great role in decreasing the cohesion and internal friction angle of the soil mantle and rock units.

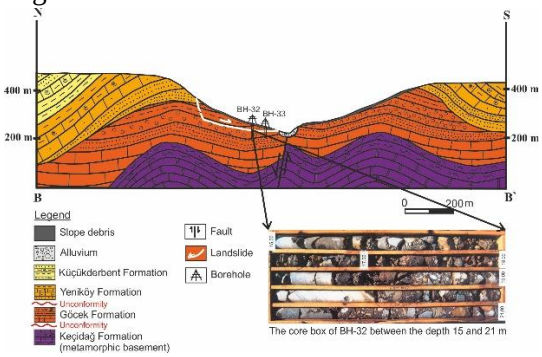

Figure 1. The geological setting of the reservoir slopes (revised from Kadakci Koca and Koca 2019)

Conclusion

The topographical evolution between 1953 and 2017 together with the mechanical and structural evolution of rock and soil units derived from back analyses gave the insight to understand the multi-temporal evolution of slope materials in a geotechnical manner. In addition, the determined fluctuations in movement rates were attributed to factors such as precipitation, fire incidents, and seismic events. However, a shorter period of differential DEMs that coincide pre-event and post-event is required for a more precise estimation of triggering factors. Hence, the landslides due to the triggering factors can not be evaluated as co-event or post-event. Overall, the study sheds light on the complex interplay of geological, hydrogeological, and geotechnical factors influencing landslide dynamics, providing valuable insights for future risk mitigation strategies in similar environments.

References

Gan, B.; Yang, X.; Zhou, J. GIS-based remote sensing analysis of the spatial-temporal evolution of landslides in a hydropower reservoir in southwest China. *Geomatics, Natural Hazards and Risk.* 2019, 10(1), 2291-2312.

International Society for Rock Mechanics (ISRM). R. Ulusay; J. A. Hudson, (Eds.). *The complete ISRM suggested methods for rock characterization, testing and monitoring: 1974-2006*. Kozan Ofset: Ankara, Türkiye, 2007.

Iqbal, J.; Tu, X.; Xu, L. Landslide Hazards in Reservoir Areas: Case Study of Xiangjiaba Reservoir, Southwest China. *Natural Hazards Review*. 2017, 18(4), 040170009.

Kadakci Koca, T. *Multi-Temporal Stability Investigation of Landslides in Çağlayan Dam Reservoir Area*. Ph.D. Thesis, Dokuz Eylül University, İzmir, Türkiye, 2021.

Kadakci Koca, T; Koca, M.Y. Volume estimation and evaluation of rotational landslides using multi-temporal aerial photographs in Çağlayan dam reservoir area, Turkey. *Arabian Journal of Geosciences.* 2019, 12, 140.

Kafle, L.; Xu, W.; Zeng, S.; Nagel, T. A numerical investigation of slope stability influenced by the combined effects of reservoir water level fluctuations and precipitation: A case study of the Bianjiazhai landslide in China. *Engineering Geology*. 2022, 297, 106508.

landslide in the Three Gorges Reservoir region under the combined effect of reservoir water level fluctuation and rainfall. *Engineering Geology*. 2016, 205, 133-145.

Luo, S.; Jin, X.; Huang, D. Long-term coupled effects of hydrological factors on kinematic responses of a reactivated landslide in the Three Gorges Reservoir. *Engineering Geology*. 2019, 261, 105271.

Sun, G.; Zheng, H.; Huang, Y.; Li, C. Parameter inversion and deformation mechanism of Sanmendong

Wang, W.; Wang, P.; Zhang, Z. Study on gravel soil strength degradation and its influence on the slope stability in reservoir bank fluctuating zone. *Engineering Failure Analysis*. 2022, 134, 105980.

3D-NUMERICAL SIMULATION OF GEOMECHANICAL FRACTURE PROCESSES IN THE VICINITY OF DEEP GEOTHERMAL DRILLINGS IN SE BAVARIA, GERMANY

JUSTIN MATTHEIS[1], CATHARINA DREXL[2], PATRICIA AMBOS[3], KUROSCH THURO

[1] *Technical University of Munich, Chair of Engineering Geology, Germany, justin.mattheis@tum.de*

[2] *Technical University of Munich, Chair of Engineering Geology, Germany, catharina.drexl@tum.de*

[3] *Technical University of Munich, Chair of Engineering Geology, Germany, patricia.ambos@tum.de*

[4] *Technical University of Munich, Chair of Engineering Geology, Germany, thuro@tum.de*

Introduction

In SE Germany, the well-known hydro-geothermal reservoir in the North Alpine Foreland Basin (NAFB) provides a suitable renewable source for domestically and industrially demanded heat (Agemar et al., 2014). However, the reservoir, i.e., carbonates reaching up to 5 km deep below the surface, shows widely known heterogeneity. Its varying hydraulic and mechanical properties constitute risks for the efficient planning and execution of these wells. Increasing the understanding of subsurface processes is a crucial task to significantly expand the share of geothermal heat supply in the heating sector. Besides the acting stress conditions, the geomechanical behavior of these deep wells is highly dependent on mechanical rock mechanical properties and the orientation of discontinuities such as faults and joints.

Methods

3D-numerical models are created using the hybrid FDEM code "Irazu" (Geomechanica Inc., Canada) to investigate the fracture process zone around a vertical wellbore, dissected by oblique joint sets. Mattheis et al. 2023 defined three typical lithologies for the carbonate reservoir and assigned typical rock mechanical parameters. Additional fracture energy testing by Ambos (2024), according to the experiments described in Kuruppu et al. (2014, mode I) and Bahrami et al. (2020, mode II) led to updated values for the "Limestone" and "Dolostone" material and completes the material parameters used for the simulations in Tab. 1. All other numerical parameters were kept at a default, and the stress tensor for the investigated depths of three to five kilometers was calculated after Potten (2020). In contrast to previous 2D FDEM models (Mattheis et al. 2023, Stockinger 2022) the three-dimensional stress tensor could be applied. The discontinuity (DFN) properties and orientations were adopted from Stockinger (2022). The model is initialized with the in-situ stress state and after 50% of timesteps the borehole excavation is simulated by reduction of the cores Young's modulus. In total, 18 3D models were simulated (nine with and nine without DFN).

Table 1. Experimentally determined material parameters used in the numerical models.

Material	Density	Young's modulus	Poisson's ratio	Tensile Strength	Cohesion	Coefficient of friction	Fracture Energy I	Fracture Energy II
	ρ_b [g/m^3]	E [GPa]	ν [-]	σ_t [MPa]	c [MPa]	μ [-]	G_{CI} [N/m]	G_{CII} [N/m]
Limestone	2.61[2]	42.96[2]	0.15[2]	5.60[2]	18.00[4]	0.6[4]	28.04[3]	133.00[1]
Strong Limest.	2.63[2]	49.44[2]	0.14[2]	10.10[2]	31.00[4]	0.6[4]	48.50[1]	243.90[1]
Dolostone	2.67[2]	52.96[2]	0.09[2]	10.10[2]	20.00[4]	0.6[4]	25.24[3]	111.90[3]

Notes: [1] after Mattheis et al. (2023); [2] after Potten (2020); [3] after Ambos (2024), [4] estimated by Irazu

Results

In general, fractured elements (= generated fractures) appear for all materials and originate from the wellbore wall. With increasing depth and, therefore, stress magnitude, the fractures penetrate deeper into the rock mass. As shown in Figure 1, the integrated joint sets weaken first, as their frictional and cohesive properties are lowest in the rock mass. Wedge-shaped breakouts form the wellbore wall and are in the direction of the least principal stress (Shmin). Although most of the fractures form after the

excavation, especially near the joints, fracturing also occurs before due to the time-dependent, stepwise reduction of Young's modulus before excavation. The "Limestone" constitutes the weakest material, and the "Strong Limestone" showed the most minor extent of fracturing, being the toughest material. A sensitivity study showed that the fracture energy parameters influence the occurring fracture pattern the most.

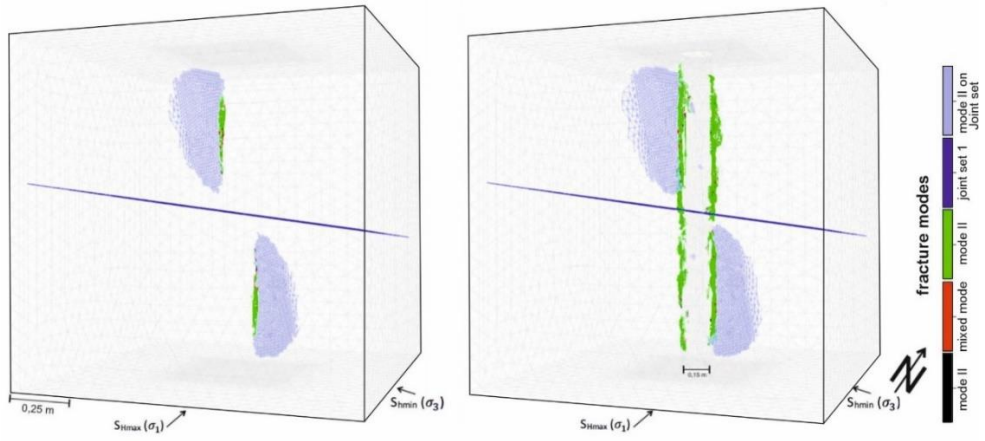

Figure 2. Fracture formation and occuring fracture modes of material "dolostone" with joint sets in 5 km. left: fracturing shortly before excavation, right: fractures after excavation, modified after Ambos (2024)

Conclusion

The modeled results show the importance of constraining the numerical results with experimentally determined input parameters, as especially the fracture energies vary significantly depending on the rock type and are, additionally, two of the most essential input parameters controlling the model's stability. The 3D-numerical models show potentially problematic scenarios regarding breakout formation and show that in-situ stresses, lithologies, and DFNs control fracture propagation. In contrast with the 2D results from Mattheis et al. 2023, it was found that discontinuities in the rock mass promote breakouts and increased fracture propagation and thus have a negative influence on borehole stability. Also, the 3D-modeled scenarios produced generally fewer fractures than the models of Mattheis et al. (2023). Expanding the models to more diverse scenarios, including deviated wells and further comparison of 2D and 3D results, is necessary to understand the subsurface conditions around the deep geothermal wells and is, thus, the subject of future work.

References

Agemar, T.; Weber, J.; Schulz, R. Deep Geothermal Energy Production in Germany. *Energies*, 2014, 7(7), 4397–4416.

Ambos, P. *Dreidimensionale geotechnische FEMDEM Modellierung eines Bohrlochs in einem tiefgeothermalen Reservoir des süddeutschen Molassebeckens.* unpubl. Master's Thesis, Technical University of Munich, Munich, 2024.

Bahrami, B.; Nejati, M.; Ayatollahi, M.; Driesner, T.; Bahramit, B. Theory and experiment on true mode II fracturing of rocks. *Engineering Fracture Mechanics*, 2020, 240(1).

Kuruppu, M.D.; Obara, Y.; Ayatollahi, M.R.; Chong, K.P.; Funatsu, T. ISRM-Suggested Method for Determining the Mode I Static Fracture Toughness Using Semi-Circular Bend Specimen. *Rock Mechanics and Rock Engineering*, 2014, 47(1), 267–274.

Mattheis, J.; Drexl, C.; Potten, M.; Stockinger, G.; Thuro, K. Borehole stability in geothermal reservoirs - A combined laboratory and numerical approach. 2023*, Proceedings of the 15th ISRM Congress 2023 & 72nd Geomechanics Colloquium*.

Potten, M. *Geomechanical characterization of sedimentary and crystalline geothermal reservoirs*. Ph.D. Thesis. Technical University of Munich, Munich, 2020.

Stockinger, G. *Fracturing in Deep Boreholes*. Ph.D. Thesis. Technical University of Munich, Munich, 2022.

VIRTUAL OUTCROP RECONSTRUCTION FOR HYDROGEOLOGICAL PARAMETRIZATION (DARUVAR, CROATIA)

IVAN KOSOVIĆ [1], MARCO POLA [1], JOSIP TERZIĆ [1], KOSTA URUMOVIĆ [1], STAŠA BOROVIĆ [1], TIHOMIR FRANGEN [1], MIRJA PAVIĆ [1], BOJAN MATOŠ [2], IVICA PAVIČIĆ [2], ANDREA BISTACCHI [3], SILVIA MITTEMPERGHER [3], STEFANO CASIRAGHI [3], GABRIELE BENEDETTI [3]

[1] *Croatian Geological Survey, Sachsova 2, Zagreb, Croatia; corresponding author: ikosovic@hgi-cgs.hr*

[2] *University of Zagreb, Faculty of Mining, Geology and Petroleum Engineering, Pierottijeva 6, Zagreb, Croatia*

[3] *University of Milan – Bicocca, Department of Earth and Environmental Sciences, Piazza della Scienza 4, Milano, Italy*

Introduction

Geothermal resources are crucial within the ongoing green energy transition because they are renewable sources of energy and raw materials. Site-specific plans based on geological and hydrogeological reconstructions are required for their preservation. Deep carbonates host important geothermal resources (Goldscheider et al., 2010), and Croatia is rich in such geothermal resources. The occurrence of thermal waters in the town of Daruvar (Figure 1A) has been extensively investigated. Thermal springs (temperatures of 38-50°C) are the outflow area of an intermediate scale hydrothermal system hosted in a fractured Mesozoic carbonate aquifer (Kosović et al., 2024). In this research, structural analyses, hydrogeological investigations, and discrete fracture network (DFN) modeling were conducted for the structural and hydrogeological characterization of the Daruvar thermal aquifer.

Methods

- Structural investigations were conducted NE of Daruvar (red square in Figure 1A) where the carbonate rock complex is exposed. They included the measurement of the main discontinuity sets and the photogrammetric reconstruction of delineated outcrops. The digital outcrop model allowed collecting a large dataset of discontinuities for the statistical analysis of their geometry (e.g., Bistacchi et al., 2020).
- Hydrogeological investigations allowed to quantify the porosity (Φ) and permeability (k) of the thermal aquifer based on the well log and pumping test of a 190 m deep well in Daruvar. Well logging was conducted after the drilling in 2008, while the pumping test was performed in 2022. The results were analyzed using classical approaches for the interpretation of pumping tests (Hantush, 1961).
- DFN modeling was used to constrain the hydrogeological parametrization of the aquifer. A model at the scale of the carbonate aquifer explored by hydrogeological investigations (Figure 1B) was constructed and calibrated using the results of structural and hydrogeological analyses.

Results

702 images were acquired resulting in a sub-cm digital outcrop model of 0.2 km^2. Virtual structural analysis depicted two dominant systems of discontinuities dipping towards N241°of 65° and N296° of 75 that reflected measured bedding and fracture sets from field investigations. A highly fractured section of the outcrop, likely similar to the intensely fractured aquifer, was selected for the statistical analysis of the geometrical features of the discontinuity sets to derive the input parameters for the DFN modeling.

Using the results of caliper log, a section of the well with tight walls was considered as representative of the natural aquifer condition. The resulting Φ from the neutron log was from 0.03 to 9.1% (average = 2.7%). The k was calculated using transmissivity values from the pumping test analyses and literature (Borović et al., 2019). Different aquifer thicknesses (investigated thickness, saturated thickness, thickness of fracture corridors) were considered resulting in a k from 7.4 to 122.8 D (average = 46 D).

The two discontinuity sets identified by structural investigations were reproduced into the DFN model. The model calibration mostly explored the discontinuity aperture. This parameter was not measured on the field because it would not be representative of the aquifer situation at depth due to the surficial relaxation of the rock mass. The result of the calibration was a linear and power correlation of the aperture with Φ and k, respectively. Considering the average Φ of the aquifer, the calibrated aperture

value was 3 mm obtaining a k value of 1.5×10^5 D. Such high k was interpreted as connected to the Φ used for the calibration, which represents the total Φ. Fluid flow is influenced by the effective Φ, which is at least an order of magnitude lower than total Φ in carbonate aquifers. This difference was accounted for by testing a "dual aperture" approach. Considering the experimental dataset, a Φ of 0.2% (10^{th} percentile of the distribution) was tested. It resulted in a calibrated fracture aperture of 0.22 mm obtaining a k of 60.5 D (Figure 1C), comparable with the experimental dataset.

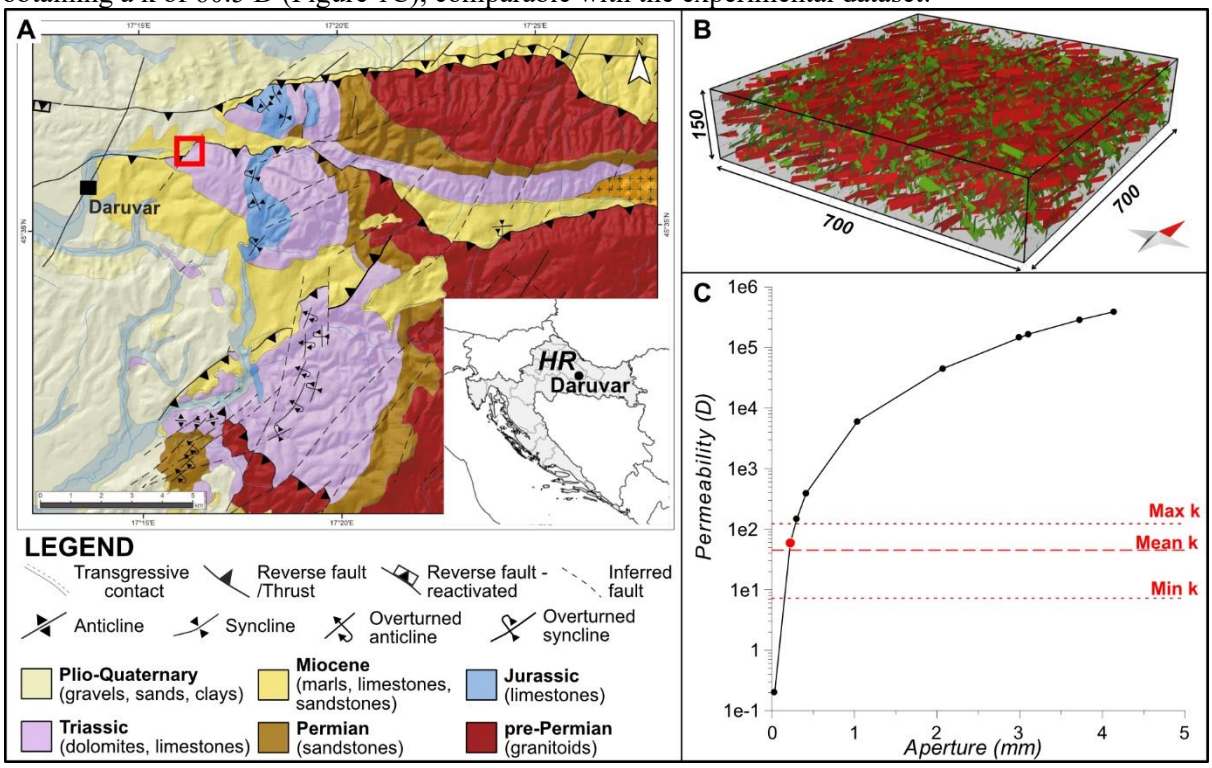

Figure 1. (A) Simplified geological map. (B) Aquifer scale DFN model. (C) The best DFN model (aperture of 0.22 mm) resulted in comparable calibrated and experimental permeability values (red dot and lines).

Conclusion

The obtained results highlight the importance of integrating structural and hydrogeological approaches to investigate fractured aquifers. Structural data can be used to determine the architecture of the fracture network in the rock mass, while hydrogeological investigations supported by numerical modeling calibrated from structural results can provide a solid hydrogeological parametrization of the aquifer.

Acknowledgments

This research was funded by the HyTheC project of HRZZ, grant number UIP-2019-04-1218.

References

Bistacchi, A.; Mittempergher, S.; Martinelli, M.; Storti, F. On a new robust workflow for the statistical and spatial analysis of fracture data collected with scanlines (or the importance of stationarity). *Solid Earth*, 2020, 11, 2535–2547

Borović, S.; Pola, M.; Bačani, A.; Urumović, K. Constraining the recharge area of a hydrothermal system in fractured carbonates by numerical modelling. *Geothermics*, 2019, 82, 128–149.

Goldscheider, N.; Mádl-Szőnyi, J.; Erőss, A.; Schill, E. Review: Thermal water resources in carbonate rock aquifers. *Hydrogeology Journal*, 2010, 18(6), 1303–1318

Kosović, I.; Matoš, B.; Pavičić, I.; Pola, M.; Mileusnić, M.; Pavić, M.; Borović, S. Geological modeling of a tectonically controlled hydrothermal system in the southwestern part of the Pannonian basin (Croatia). *Frontiers in Earth Science*, 2024, 12, 1401935.

Hantush, M.S. Aquifer Tests on Partially Penetrating Wells. *Journal of the Hydraulics Division*, 1961, 87, 171–195.

SURFACE GEOPHYSICAL INVESTIGATION OF NATURAL THERMAL SPRING AREA IN DARUVAR, CROATIA

MARCO POLA [1], IVAN KOSOVIĆ [1], JOSIP TERZIĆ [1], KOSTA URUMOVIĆ [1], BOJAN MATOŠ [2], STAŠA BOROVIĆ [1]

[1] *Croatian Geological Survey, Sachsova 2, Zagreb, Croatia, mpola@hgi-cgs.hr,*

[2] *University of Zagreb, Faculty of Mining, Geology and Petroleum Engineering, Pierottijeva 6, Zagreb, Croatia, bojan.matos@rgn.unizg.hr*

Introduction

Renewable geothermal resources play an important role in the green global energy transition. A key factor for estimating the potential of a geothermal resource is a detailed reconstruction of the architecture of the aquifer and the geological setting in the outflow area favoring the upwelling of thermal waters. Croatia is rich in geothermal resources and the occurrence of thermal waters in Daruvar city has been extensively investigated (e.g., Borović et al., 2019; Kosović et al., 2023). This research focuses on the local scale reconstruction and modeling of the geological setting of the Daruvar thermal spring area using an integrated geophysical approach based on electrical resistivity tomography and both active and passive seismic methods.

Methods

Electrical resistivity tomography (ERT) was employed to delineate the structural and lithological properties of the Daruvar spring area. Eight profiles were acquired using an electrical imaging system in 2021 and 2022. Field apparent resistivity data were inverted into 2D resistivity subsurface models reconstructing the geometries of lithologies and structures in the subsurface (Loke et al., 2013). An integrated approach based on the active multichannel analysis of surface waves (MASW) and the passive horizontal-to-vertical spectral ratio (HVSR) methods was applied to map the thickness of the Quaternary cover. The center of the MASW seismic profile was located where the 6 stations of HVSR measurement were conducted. The seismic impedance contrast between bedrock and unconsolidated Quaternary sediments creates a peak in the H/V curve (ratio of horizontal to vertical seismic noise spectra), which was used to estimate the thickness of the alluvial cover (Nakaruma, 2019). The thickness calculation depends on the vertical distribution of the surface waves' velocity, which was assessed using the MASW approach for a site-specific reconstruction (Park et al., 1999).

Results

The spatial distribution of resistivity shows relatively low values from 10 to 150 Ωm (Figure 1). Based on the stratigraphic logs of the wells, three resistivity layers/geological units were identified (Figure 1): (1) the Quaternary alluvial cover with resistivity ranging between 30 and 50 Ωm (layer 1); (2) the Neogene sediments with resistivity values of 10-30 Ωm (layer 2); and (3) the Triassic dolomites that were divided in a compact layer with resistivity ranging from 70 to 150 Ωm (layer 3a) and a fractured layer characterized by resistivity values of 20-30 Ωm (layer 3b). Furthermore, sharp lateral variations in the resistivity distributions were observed. They were generally marked by low resistivity anomalies and were interpreted as fracture zones along the faults (dashed red lines in Figure 1). The high secondary porosity of the fracture zones, which was connected to their intense fracturing, and the occurrence of thermal waters decreased the bulk resistivity of the rock mass.

The obtained results allowed us to reconstruct the architecture and geological properties of the Daruvar thermal spring area. The Quaternary cover has a thickness of 5 to 15 m increasing northward and eastward. Its thickness and geometry were confirmed by the seismic investigations. Neogene deposits are generally found below the Quaternary alluvial cover, except for the central part of the study area where the Triassic dolomites are found at the surface. Two main faults border southward and eastward the thermal spring area juxtaposing the highly permeable Triassic dolomites with the low permeable Neogene deposits. This lateral contrast fosters the rising of the thermal waters forming a shallow thermal resource in the Daruvar area. The main outflow of the Daruvar thermal springs, represented by the

Antunovo vrelo, Blatna kupelj, and Ivanovo vrelo springs (A, B, and I, respectively, in Figure 1), occurs within the interaction zone of the faults imaged through ERT. Faults are associated with highly permeable damage zones that represent a preferential pathway for the circulation of thermal fluids. The connected fault zones enhance the upwelling of thermal waters resulting in the occurrence of the thermal springs with water temperature up to 48°C (Borović et al., 2019).

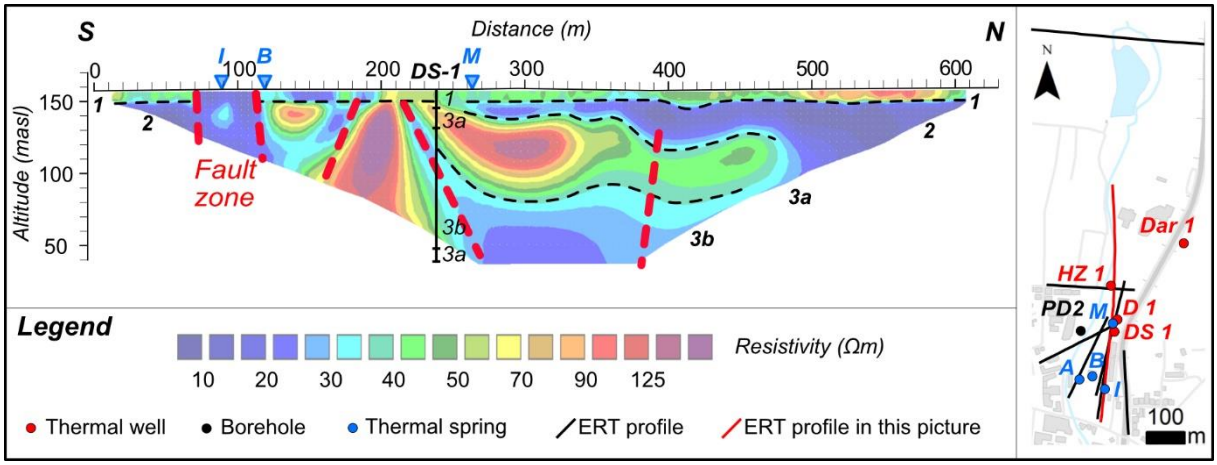

Figure 1. Inverse resistivity model of an ERT profile (red line in the map) conducted with 10 m spacing between electrodes. It shows a general overview of the resistivity distribution in the Daruvar spring area. Dashed red lines indicate fault zones characterized by low resistivity values. The map shows the traces of ERT profiles (black lines) and the locations of springs and boreholes (dots) used for the geological reconstruction.

Conclusion

This research focused on the reconstruction of the geological and structural settings of the Daruvar thermal spring area using different geophysical methods. Their joint interpretation completed with the stratigraphic logs of exploitation wells and boreholes allowed the reconstruction of the vertical and horizontal distributions of lithological units and proved the occurrence of faults deforming the bedrock in the Daruvar area. The local fault and fracture networks permit a quick upwelling of thermal fluids resulting in thermal springs with temperatures up to 48°C. This work proves that a cost-effective geophysical approach could be used to investigate shallow geothermal systems hosted in fractured carbonate rocks.

Acknowledgments

This research was funded by the HyTheC project of HRZZ, grant number UIP-2019-04-1218.

References

Borović, S.; Pola, M.; Bačani, A.; Urumović, K. Constraining the recharge area of a hydrothermal system in fractured carbonates by numerical modeling. *Geothermics*, 2019, 82, 128–149.

Kosović, Ivan; Briški, Maja; Pavić, Mirja; Padovan, Božo; Pavičić, Ivica; Matoš, Bojan; Pola, Marco; Borović, Staša. Reconstruction of Fault Architecture in the Natural Thermal Spring Area of Daruvar Hydrothermal System Using Surface Geophysical Investigations (Croatia). *Sustainability*, 2023, 15; 12134, 22.

Nakamura, Y. What Is the Nakamura Method? Seismol. Res. Lett. 2019, 90, 1437–1443.

Park, C.B.; Miller, R.D.; Xia, J. Multichannel Analysis of Surface Waves. Geophysics 1999, 64, 800–808.

3D RANDOM FIELD MODELLING OF SUBSURFACE STRATIGRAPHY AND GEOTECHNICAL PARAMETERS IN THE TAIPEI BASIN: IMPLICATIONS FOR MAPPING V_{S30}

STEFAN CHRISTOPHER NICHOLAS[1], JIA-JYUN DONG[2], YU-CHEN LU[3]

[1] PhD Candidate, Graduate Institute of Applied Geology, National Central, University, Taiwan, stefan_nicholas@hotmail.co.uk

2 Professor, Graduate Institute of Applied Geology, National Central, University, Taiwan, jjdong@geo.ncu.edu.tw

3 Postdoc, Graduate Institute of Material Sciences and Engineering, National Central, University, Taiwan, erwin92302101@hotmail.com.

Introduction

Seismic hazards are a significant challenge in Taiwan, especially in the Taipei Basin, which is particularly vulnerable due to site effects and its high population density. Covering an area of around 243 km², the Taipei Basin's top 30 meters mainly consists of alternating layers of sand and clay from the Sungshan Formation, and in some areas towards the basin margins, the underlying Jingmei Formation, which is composed of alluvial gravel. The average shear-wave velocity of the upper 30 meters of the ground (V_{S30}) is commonly used to assess site effects (Anderson et al. 1996; Park and Elrick 1998; Huang et al. 2007; Tsai et al, 2021), caused by soft alluvial sediment overlying hard rock, resulting in amplified shear-waves and intensified ground motion (Kuo, 2011). This creates the need for an accurate regional scale V_{S30} map for the Taipei Basin. Previous studies on V_{S30} mapping in the Taipei Basin have primarily relied on interpolation methods, such as Kriging, to generate V_{S30} maps (Lee and Tsai, 2008). However, these approaches often overlook the impact of geological and geotechnical model uncertainty on V_{S30} estimation, resulting in maps that may not fully capture the spatial variability of geological and geotechnical properties. To address this issue, we utilised a stratigraphic based geo-property random field model (SGRF) (Lu et al., 2024) to produce probabilistic stratigraphic and geotechnical parameter models and assess the associated uncertainties. In the SGRF model, stochastic Markov random field (SMRF) (Li et al., 2016; Wei and Wang, 2022; Lu et al., 2024) provides the probabilistic framework for the geological model. After the geological model is established, geotechnical parameter models for unit weight and void ratio are developed using fractional Brownian motion (fBM). These models are subsequently used to generate shear-wave velocity models, which are then employed to calculate V_{S30}. After multiple realisations, the mean and standard deviation of V_{S30} is used quantify the spatial variability and uncertainty.

Methods

The workflow for this study is outlined in Figure 1. First, data from 6,804 boreholes was collected and screened, including stratigraphic configurations, unit weight, and void ratio. Following this, an initial geological model was simulated utilizing SMRF theory (Li et al., 2016; Wei and Wang, 2022; Lu et al., 2024). This involves establishing a neighbor system and simulation order, followed by performing Markov Chain Monte Carlo (MCMC) simulations to produce multiple potential realizations of the subsurface stratigraphy, enabling the quantification of uncertainty through the principle of information entropy. Bayesian machine learning calibrates the parameters of the SMRF model based on the probability of correctly predicting soil layers in observation wells from each MCMC simulation (Lu et al., 2024). Subsequently, geotechnical parameter models are simulated using fractional Brownian motion (fBM). This starts with determining the spatial probability of geotechnical parameters within a neighbor system based on the geological model. Once the neighbor system, spatial probability, simulation order, and standard deviation spatial matrix have been established, MCMC simulations are then performed. Statistical values of geotechnical parameters for each soil layer from each MCMC simulation are used with Bayesian machine learning to calibrate parameters of fBM. Shear-wave velocity (Vs) models are calculated using Vs estimation functions that correlate vertical effective stress (calculated from the unit weight models and groundwater level data) and void ratio to Vs for different

soil types. The mean and standard deviation of Vs across the Taipei Basin are then calculated after 500 realisations. Finally, a V_{S30} distribution map is created based on the mean Vs in the top 30 m of the ground, and the V_{S30} uncertainty is compared to the geological model uncertainty.

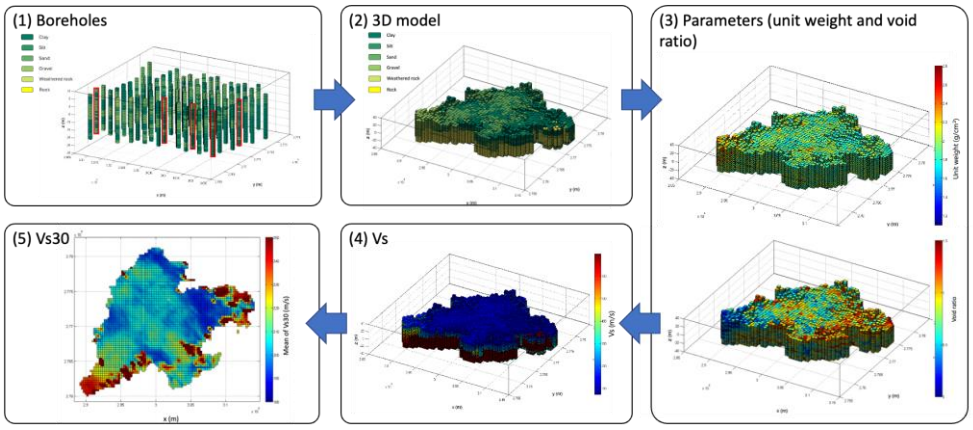

Figure 1. Research workflow; (1) digitalize borehole data, (2) generate 3D Markov random field-based geological model, (3) create geotechnical parameter models using Fractional Brownian Motion, (4) generate shear wave velocity (Vs) models using estimation functions that correlate Vs to void ratio and vertical effective stress, (5) produce V_{S30} map for the Taipei Basin.

Results

According to the results, the majority of the region's V_{S30} values range from approximately 190 to 220 m/s, which aligns with measured V_{S30} values from strong motion stations within the basin. While at the southern and eastern boundaries of the study area, V_{S30} values rise to around 250 m/s, which is also observed in the measured data. Compared with previous V_{S30} maps within the Taipei Basin, such as by Lee and Tsai 2008, our results show a similar trend but with key differences in more localised areas. For example, our study identifies larger low V_{S30} areas (<180 m/s) in the north and northeast of the basin, which are critical for seismic hazard assessments. The results also show that the shear-wave velocity distribution is closely correlated to the different geological layers, and areas with higher geological model uncertainty also exhibit higher uncertainty in V_{S30}. This is shown in Figure 2, where the average information entropy in the top 30 m of the ground ($I_{E,30}$), which is used to quantify the uncertainty in the geological model, is compared to the standard deviation of the V_{S30} map.

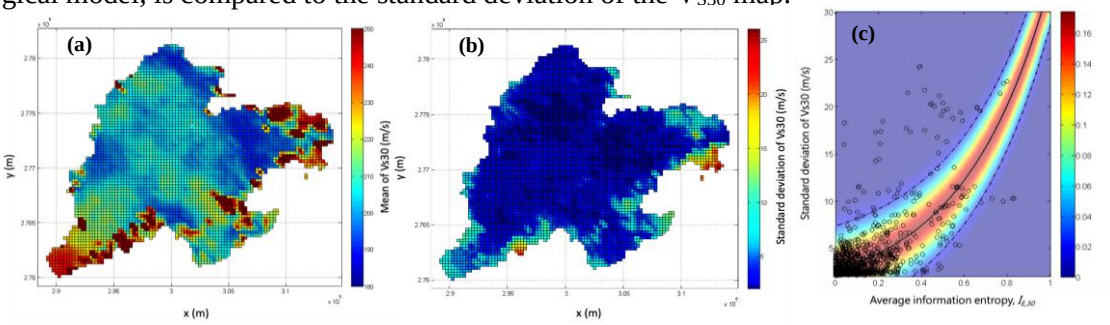

Figure 2. (a) Mean of V_{S30} in the Taipei Basin after 500 realisations, (b) standard deviation of V_{S30} in the Taipei Basin after 500 realisations, (c) relationship between uncertainty in the geological model and standard deviation of V_{S30}.

Conclusion

This study utilises a probabilistic framework to estimate V_{S30} in the Taipei Basin, while considering the spatial distribution of geological layers and geotechnical parameters. The findings emphasize the critical importance of considering geological model uncertainty when calculating V_{S30}, Furthermore, the random field method offers several advantages over traditional geostatistical methods by directly considering the spatial distribution characteristics of the subsurface stratigraphy.

References

Anderson, J. G., Lee, Y., Zeng, Y., and Day, S. (1996). Control of strong motion by the upper 30 meters, Bull. Seismol. Soc. Am. 86, 1749–1759.

Huang, M. W., Wang, J. H., Ma, K. F., Wang, C. Y., Hung, J. H., and Wen, K. L. (2007). Frequency-dependent site amplifications with f ≥ 0:01 Hz evaluated from the velocity and density models in Central Taiwan, Bull. Seismol. Soc. Am. 97, 624–63

Kuo, C. H., Wen, K. L., Hsieh, H. H., Chang, T. M., Lin, C. M., & Chen, C. T. (2011). Evaluating empirical regression equations for VS and estimating VS30 in northeastern Taiwan, Soil Dynam. Earthq. Eng. 31, 431–439.

Lee, C. T., and Tsai, B. R. (2008). Mapping VS30 in Taiwan, Terr. Atmos. Ocean. Sci. 19, 671–682.

Li, Z., Wang, X., Wang, H., and Liang, R.Y. (2016). Quantifying stratigraphic uncertainties by stochastic simulation techniques based on Markov random field, Eng. Geol. 201, 106–122.

Lu, Y. C., Chien, W. Y., Nicholas, S. C., Dong, J. J., Juang, C. H., and Tien, Y. M. (2024). Three-dimensional probabilistic geological and geotechnical property modeling. Geotech 2024 (TGS), 26-28 Aug., Tainan, Taiwan.

Park, S., and Elrick, S. (1998). Predictions of shear-wave velocities in southern California using surface geology, Bull. Seism. Soc. Am. 88, 677– 685.

Tsai, C. C., Kishida, T., & Lin, W. C. (2021). Adjustment of site factors for basin effects from site response analysis and deep downhole array measurements in Taipei, Eng. Geol. 285, 106071.

Wei, X., and Wang, H. (2022). Stochastic stratigraphic modeling using Bayesian machine learning, Eng. Geol. 307, 106789.

FROM DATA TO DEPTHS: A JOURNEY INTO 3D GEOLOGICAL MODELLING

LUCIE BAUDOUY [1], ANNA FIORAVANTI [1], CEDRIC DUVAIL [1]

[1] *Ginger CEBTP, France,* c.duvail@groupeginger.com

Introduction

In this extended abstract, we present the general methodology employed by our geological consulting team to deliver 3D geological models to our clients across various thematic areas. Our approach involves applying agile methods, utilizing disparate data of varying quality and sources, to provide cost-effective and time-efficient models that meet the study's requirements.

Methods

The development of a 3D subsurface model is a multifaceted process that demands a structured approach. The methodology encompasses several critical stages, each contributing to the accuracy and utility of the final model. Herein, we present an outline of the essential steps involved in this process.

The foundation of any reliable 3D subsurface model lies in the comprehensive collection and meticulous preparation of relevant data. Geological maps, field surveys, borehole logs, and geophysical survey results constitute the primary data sources. The precision of these data sets directly impacts the quality of the model, requiring rigorous validation and calibration to ensure their reliability and coherence.

Identifying the geological units to be represented in the model is a critical task. This step requires a detailed analysis of the collected data to discern the various geological formations present within the study area. The differentiation of these units is based on their lithological, structural, and geotechnical characteristics, which are essential for constructing an accurate and functional model. The clear identification and delineation of these units is imperative for the subsequent modelling processes.

The prepared data are then imported into specialized 3D modelling software, such as Leapfrog Works. This stage involves ensuring that the data is correctly formatted and compatible with the software's requirements. The integrity of the data during importation is essential, as any discrepancies or errors can propagate through the modelling process, potentially compromising the model's accuracy.

After the data import, the next step is the creation of the 3D subsurface model by constructing a three-dimensional representation of the subsurface geological units. The software employs advanced interpolation techniques to generate continuous surfaces that define the boundaries between different geological formations. This step is iterative, with continuous refinements made to improve the fidelity of the model based on the input data.

The verification and adjustment stage is critical for ensuring the model's accuracy. This involves comparing the model's output with the original field data and making necessary adjustments to rectify any inconsistencies. The use of validation techniques, such as cross-validation with independent data sets, enhances the reliability of the model. This stage may require multiple iterations to achieve a model that accurately represents the subsurface conditions.

Results

Geological modelling enables spatial visualization and representation of geological units and formation geometries. This approach is important for engineers and infrastructure designers to better understand the nature and distribution of geological materials in subsurface environments. It also facilitates the estimation of physical properties distribution such as strength, permeability, and density, which are essential for assessing the mechanical behaviour of materials and incorporating these parameters into structural design.

By modelling various geological units and considering their geotechnical characteristics, geological modelling also **assesses geotechnical risks associated** with urbanization and infrastructure development (Fioravanti and Ricard, 2022). It helps **identify potentially problematic areas**, such as **zones prone to landslides**, **differential settlements**, or **underground cavities** (Duvail *et al.* 2021).

Groundwater management benefits significantly from geological modelling by enhancing understanding of groundwater reservoirs' geometries and distributions (Duvail *et al.* 2018).

Moreover, geological modelling provides essential input data for simulating **site effects in seismic hazard** assessment (Fioravanti and Ricard, 2024). It predicts local amplification phenomena of seismic intensity, duration, and damage caused by seismic waves, critical for siting facilities like power plants, dams, or storage facilities that require precise identification of the depth to bedrock.
Lastly, it aids in estimating the **nature of rocks for excavation**, contributing to effective planning, material re-employment and management of underground infrastructure.

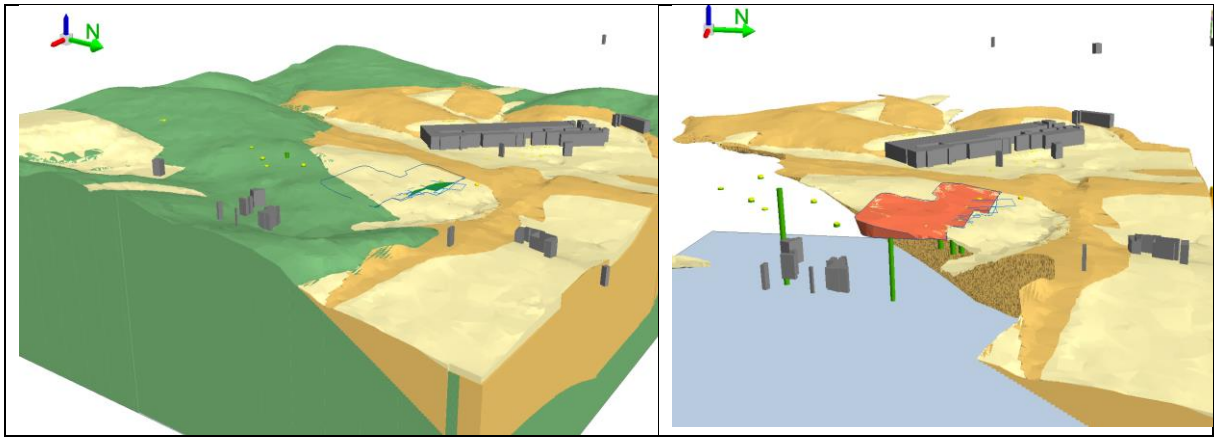

Figure 1. Example of a geological model built to estimate the volume of different materials (soft sediments versus bedrock) to be excavated (Duvail *et al.* 2022)

Conclusion

Our comprehensive methodology for developing 3D geological models showcases the integration of diverse data sources through agile and cost-effective practices. By systematically collecting, preparing, and validating geological, geotechnical, and geophysical data, we ensure the creation of accurate and reliable subsurface models. These models are indispensable tools for engineers and infrastructure designers, providing significant insights into the spatial distribution and physical properties of geological units. They also play a vital role in assessing geotechnical risks, managing groundwater resources, and evaluating how a site's geologic conditions will respond to seismic shaking. Additionally, our models optimize survey campaigns by identifying the most relevant areas for data collection, ensuring that survey efforts are both efficient and effective. Ultimately, our approach facilitates informed decision-making and enhances the planning and management of various infrastructure projects. The geological model also constitutes a useful and comprehensive discussion support between the various stakeholders and decision-makers. As we continue to refine our techniques and incorporate new data, our models will become even more precise, further supporting the successful execution of diverse geotechnical and engineering studies.

References – Few examples of main projects

Fioravanti A., Ricard B., Le Havre Wind turbines factory Extension B115, *Siemens Gamesa Renewable Energy* - France – 2024

Duvail C., Baudouy L., Fioravanti A., Update of the Cadarache geological model around the INB56 facility, France, 2022

Fioravanti A., Ricard B., Technip – Eastman - Saint Jean de Folleville, Construction of a new plant on the banks of the Seine, *Eastman Sequel project*, France, 2022

Duvail C., Baudouy L., Fioravanti A., 3D modelling of the salt cavities of la Madeleine, *Rhodia Chimie*, France, 2021

Duvail C., Baudouy L., Fioravanti A., 3D geological modelling for the management of the aquifers in Argens valley (Var). *Syndicat de l'Eau du Var Est (SEVE)*, France 2018